Reprinted from LANGMUIR, 1988, 4, 867.

In Situ Optical Structure Factor Measurements of an Aggregating Soot Aerosol

H. X. Zhang, C. M. Sorensen,* E. R. Ramer, B. J. Olivier, and J. F. Merklin

Department of Physics, Kansas State University, Manhattan, Kansas 66506

Received December 1, 1987. In Final Form: March 22, 1988

We study the agglomerate morphology of a carbonaceous soot aerosol extracted from a premixed methane/oxygen flame during combustion by the use of real-time optical structure factor measurements and subsequent transmission electron microscope examination of the settled agglomerates. We find a fractal morphology is maintained during the agglomeration growth of the aerosol with a fractal dimension $D = 1.62 \pm 0.06$. The TEM analysis also shows this fractal morphology with $D = 1.72 \pm 0.10$. These values of D are on the low side of the range $D = 1.7$–1.9 expected from diffusion-limited cluster aggregation models.

Introduction

The aggregation of small particles to form larger particles is a major growth process in colloidal and aerocolloidal systems.[1] In recent years interest in the clustering process has been heightened by the discovery[2] that the random clusters formed during this process display a fractal morphology.[2-4] A fractal is a noncompact structure that displays a scale invariance symmetry.[5] A consequence of this symmetry leads to a useful working definition of a fractal, which is that the number of monomers N inside a sphere of radius R centered on the cluster is given by

$$N \sim R^D \tag{1}$$

In eq 1, $D < 3$ is the fractal dimension, the key parameter of the fractal structure. It has been found that D is a function of the spatial dimension[3] and the details of the growth process.[6]

The first experimental work to demonstrate the fractal nature of agglomerates was performed by Forrest and Witten, who studied aerosol particles.[2] In this paper we shall use the term "agglomerate" for a cluster of particles held together by weak van der Waals forces, whereas "aggregate" may be applied to clusters held together by partial fusion of the individual particles.[7] Since that time, considerably more experimental effort has been applied to colloidal liquids rather than aerosols. In most aerosols the initial monomer size is less than the mean free path of the gas molecules. Hence, the diffusion is no longer hydrodynamic and is therefore fundamentally different than in a colloidal liquid. Because of this and the obvious technological importance of aerosols, the morphology of aerosols particles should be studied. In the aerosol phase, in addition to the work of Forrest and Witten, studies have appeared regarding fumed silica redispersed either in a liquid or in packed powders.[7,8] A variety of results for the fractal dimension D were obtained ranging from 1.8 to 2.6. Values larger than 1.8 were thought to be a result of the sample preparation method, e.g., the packing process, and thus not inherent to the coagulation process or possibly an indication of nonuniversality. Other aerosol work includes carbonaceous soot agglomerates, which have been collected and examined with a transmission electron microscope (TEM).[9] These studies have shown soot agglomerates are fractals with $D \sim 1.7$. Hence it seems reasonable to conclude that aerosol aggregates and agglomerates do display fractal morphology with $D \sim 1.7$–1.8. None of the studies above, however, were performed in situ. Thus it is impossible to know the effects of sampling and collection on the resultant morphology.

In this paper we study the agglomerate morphology of soot particles obtained from a methane/oxygen flame and captured in a 6-L flask. The morphology was studied both by collection of the resultant agglomerates for examination with a TEM and, most importantly, by in situ optical structure factor measurements. Optical structure factor measurements have been used before to determine the fractal nature of clusters.[7,10] We have also performed

* Author to whom correspondence should be addressed.

(1) Drake, R. L. In *Topics in Current Aerosol Research*; Hidy, G. M., Brock, J. R., Eds.; Pergamon: Oxford, 1972; Vol. 3, Part 2, p 201.
(2) Forrest, S. R.; Witten, T. A. *J. Phys. A* **1979**, *12*, L109.
(3) *Kinetics of Aggregatical and Gelation*, Family, F., Landau, D. P., Eds.; North Holland: Amsterdam, 1984.
(4) *On Growth and Form*, Stanley, H. E., Ostrowsky, N., Eds.; Nijhoff: Boston, 1986.
(5) Mandelbrot, B. *The Fractal Geometry of Nature*; Freeman: San Fracisco, 1983.
(6) Weitz, D. A.; Huang, J. S.; Lin, M. Y.; Sung, J. *Phys. Rev. Lett.* **1984**, *54*, 1416.
(7) Martin, J. E.; Schaefer, D. W.; Hurd, A. J. *Phys. Rev. A* **1986**, *33*, 3540.
(8) Freltoft, T.; Kjems, J. K.; Sinha, S. K. *Phys. Rev. B: Condens. Matter* **1986**, *33*, 269.
(9) Samson, R. J.; Mulholland, G. W.; Gentry, J. W. *Langmuir* **1987**, *3*, 273.

0743-7463/88/2404-0867$01.50/0

photon correlation spectroscopy (PCS) measurements to watch the mean size grow with time during agglomeration. Our motivation has been to obtain an in situ measurement of aerosol morphology and compare it to that obtained from visual TEM inspection. We were also motivated by the fact that our system models the conditions under which soot particles released to a quiescent atmosphere during combustion would agglomerate. We find a fractal dimension of $D \simeq 1.62$–1.72 from both methods. We will also show that certain irregularities exist in the TEM analysis when eq 1 is used regarding the positioning of the center of the spheres of radius R during analysis.

Experimental Section

Flame and Sampling. Our combustion apparatus was very similar to that used by us in earlier work.[11] We burned premixed flames of methane and oxygen at atmospheric pressure on a 6-cm-diameter flat-flame burner (McKenna Products). Surrounding the water-cooled frit was a 0.5-cm-wide annular nitrogen sheath. A 15-cm-diameter steel stagnation plate was mounted 2.9 cm above the burner. The fuel mixture was 54.6% methane by volume (C/O ratio of 0.60), which was sufficiently rich to produce soot.

The soot aerosol was obtained by sampling the flame with an uncooled quartz probe, 0.4-cm i.d., with an orifice diameter of 0.05 cm. The probe was mounted vertically and lowered down into the flame through a hole in the stagnation plate. The probe was made very blunt (apex angle of 40°) to cause rapid expansion and hence quenching of the sample and to reduce plugging of the orifice by soot. The tip of the probe sampled the flame 1.2 cm above the burner surface. This is well above the reaction zone of the flame at 0.3 cm. At this position in situ light-scattering measurements of the soot particle size in the flame yield an effective diameter of 50 nm.[12] Since spherical monomeric soot particles are usually ~20 nm in diameter, some aggregation of the monomers has probably already occurred in the flame.

After a 10-min stabilization of the probe in the flame, soot from the flame was extracted into a 6-L florence flask (diameter ~ 23 cm) and the flask was flushed with the aerosol for about 2 min.

After the sampling, the flask was placed in our optical eight-channel detector. Optical structure factor measurements (described below) were performed as a function of time. Photon correlation spectroscopy (PCS) measurements were also performed to determine the mean agglomerate radius. Finally, TEM grids were placed near the bottom of the flask to collect the settling agglomerates for visual examination.

Optical Structure Factor Measurements. It can be shown that the intensity as a function of angle of waves scattered from a fractal cluster is given by[8]

$$S(q) \sim q^{-D} \tag{2}$$

In eq 2, $S(q)$ is the scattered intensity and is called the static structure factor. The scattering wave vector is $\vec{q}$, and its magnitude is given by

$$q = 4\pi\lambda^{-1} \sin(\theta/2) \tag{3}$$

where λ is the wavelength of the radiation and θ is the scattering angle. Equation 2 is valid in the regime $qR_G > 1$, where R_G is the radius of gyration of the whole agglomerate and $qa < 1$, where a is the monomer radius.

To perform optical structure factor measurements we have constructed what we call an optical eight-channel detector (OECD). It is shown schematically in Figure 1. A vertically polarized He–Ne or argon ion laser beam was incident upon the soot aerosol confined inside the flask. The eight detectors were put at angles θ of 10°, 16°, 22°, 30°, 45°, 60°, 90°, and 120° with respect to the forward direction of the beam. These angles combined with our incident wavelengths of 488 or 633 nm gave us an inverse wave vector range of 600 nm > q^{-1} > 50 nm.

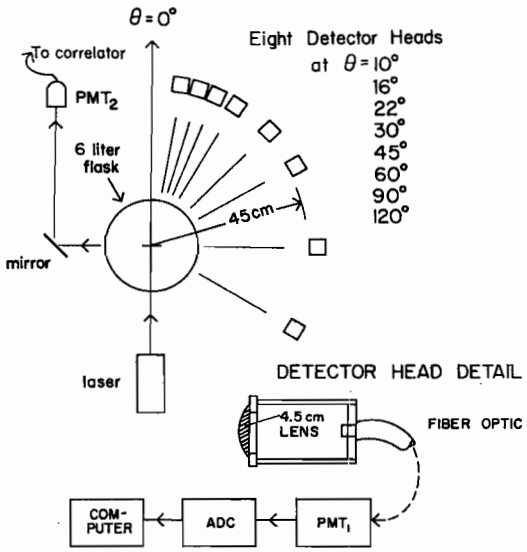

Figure 1. Schematic diagram of the optical eight-channel detector and photon correlation setup.

The detail of the detectors is also shown in Figure 1. All eight detectors used the same fiber optic cable, photomultiplier tube (PMT), and analog to digital converter for computer input and analysis. To record scattering intensity data the fiber optic was moved by hand from image zone to image zone of each of the eight detectors. Relative calibration of the eight detectors was accomplished by placing an isotropic light source in the OECD. The collection angle of the detectors was 0.7°, resulting in a relative width of the scattering vector of $\delta q/q \sim 7\%$ (for the detector at 10°) to 1% (for the detector at 90°). It can be shown that this spread in q can only affect our measurement of D by less than $^1/_2$%.

Photon Correlation Measurements. Our PCS arrangement was also very similar to that used in some of our other work.[12] Briefly, light scattered at an angle $\theta = 90°$ was collected by a lens and imaged onto a pinhole 50 cm from the cathode of an FW130 PMT. This provides good spatial coherence on the cathode and gives a good signal to noise ratio. The PMT photopulses were digitized and then passed to a commercial correlator where the intensity correlation function was computed. Analysis of this correlation function yielded the intensity-weighted mean radius of the aggregates via the equation

$$\langle I(0)I(t)\rangle = B + Ae^{-2D_{SE}q^2t} \tag{4}$$

where A and B are experimental constants, $\langle I(0)I(t)\rangle$ is the intensity correlation function, and D_{SE} is the Stokes–Einstein diffusion coefficient given by

$$D_{SE} = K_B T/(6\pi\eta R_H) \tag{5}$$

Here K_B is Boltzmann's constant, T the temperature, η the medium viscosity, and R_H the particle radius. This radius is an effective hydrodynamic radius since PCS actually measures the particle diffusion coefficient. This should be Stokes–Einstein since the agglomerate size was always much greater than the gas molecule mean free path. R_H and R_G are related by $R_H = 0.7R_G$.[13] Our purpose here was not so much a study of the mean agglomerate size but rather qualitative monitoring of the size and insuring that the conditions for $S(q)$ for eq 2 to be true were satisfied.

High-Resolution Automatic Digitizer. This digitizer consisted of a Hewlett-Packard plotter, an analog to digital converter, a computer, and an emitter–receiver sensor. This sensor was mounted in a Teflon cylinder which in turn was mounted in the penholder of the plotter. When the plotter was in the "pen down"

(10) Schaefer, D. W.; Martin, J. E.; Wiltzius, P.; Cannell, D. S. *Phys. Rev. Lett.* **1984**, *52*, 2371.
(11) Ramer, E. R.; Merklin, J. F.; Sorensen, C. M.; Taylor, T. W. *Combust. Sci. Technol.* **1986**, *48*, 241.
(12) Scrivner, S. M.; Taylor, T. W.; Sorensen, C. M.; Merklin, J. F. *Appl. Opt.* **1986**, *25*, 291.
(13) Wiltzius, P. *Phys. Rev. Lett.* **1987**, *58*, 710.

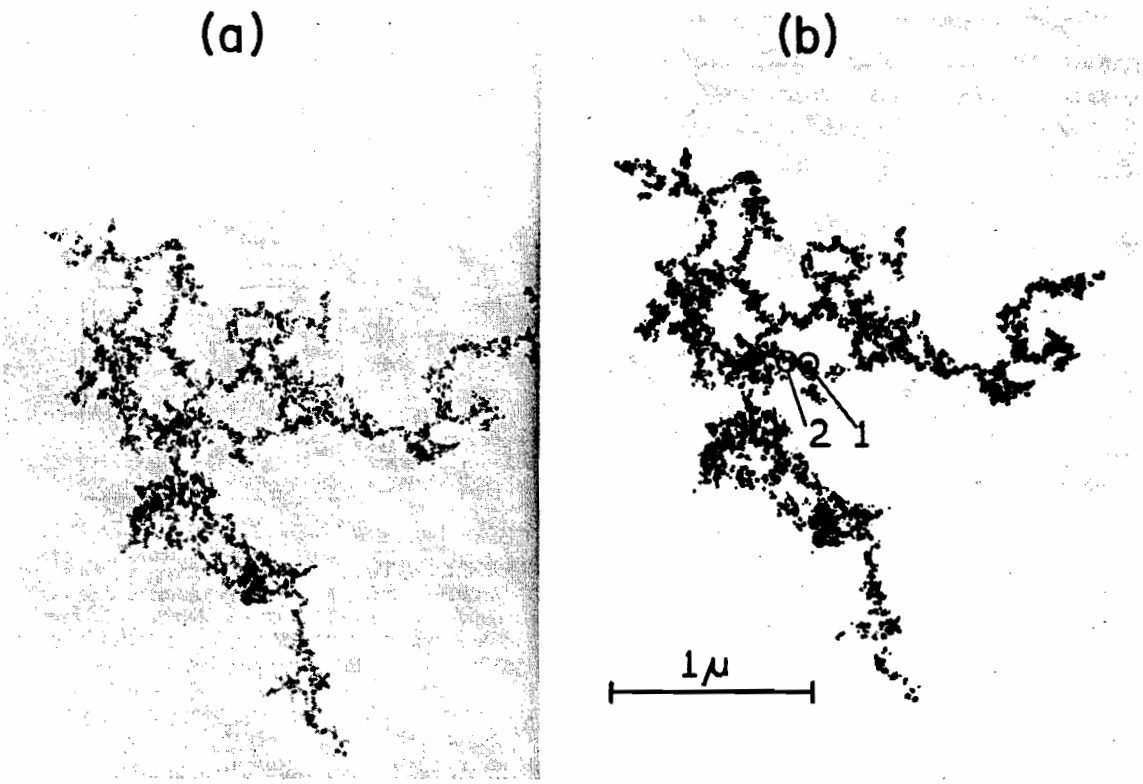

Figure 2. (a) Soot agglomerate collected by settling onto a TEM grid near the bottom of the aerosol chamber after 10 h. (b) Digitized reproduction of the soot agglomerate. Point 1 is the center of mass of the agglomerate, and point 2 optimizes the linearity of the total darkness versus radius logarithmic graph for the nested circles analysis method.

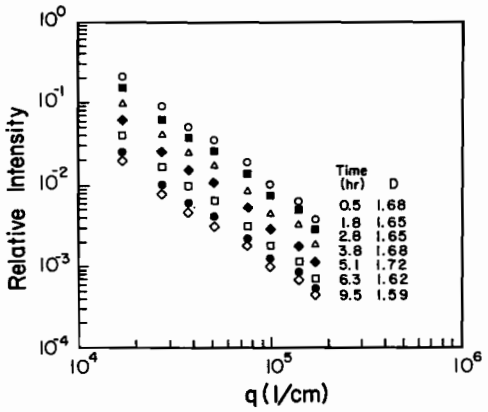

Figure 3. Relative light-scattered intensity proportional to the structure factor, $S(q)$, versus the scattering wave vector, q, for the first aerosol. Different curves are for different times after filling the flask. The average fractal dimension for all time is $D = 1.65 \pm 0.04$. The incident light had $\lambda = 633$ nm.

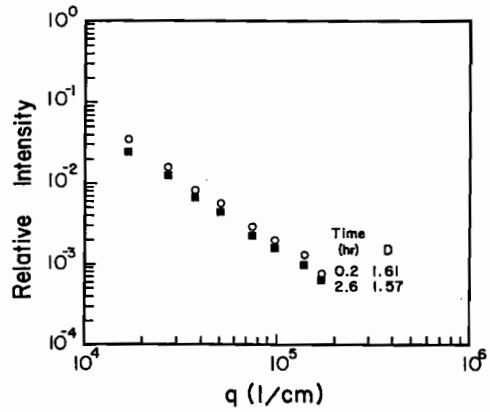

Figure 4. Second aerosol ($\sim^1/_4$ the concentration of aerosols 1 and 2). $D = 1.59 \pm 0.03$; $\lambda = 633$ nm.

configuration, this Teflon cylinder touched the TEM micrograph to be digitized. This made the sensor insensitive to room light conditions. A computer program moved the sensor device in a raster scan motion over the limits of the cluster picture. The emitter, working in the infrared, was shown locally on the TEM micrograph. The receiver then collected the reflected infrared light, and the ADC sent the signal to a computer.

The spacial resolution of this digitizer can be as high as the plotter itself, i.e., 7000 × 11 000 pixels. High resolution is necessary because the agglomerates had thousands of monomers. In practice 2000 × 3000 was sufficient. The darkness was digitized to 5000 levels.

Figure 2a shows an original picture, and Figure 2b shows the reproduced picture from its digitized image. While the darkness of the picture stored in the computer was divided into 5000 levels, the reproduced picture in Figure 2b can have only two levels, white or black, i.e., it is a binary picture. So there is a difference in principle between the pictures. However, their shapes are very alike, and Figure 2 demonstrates the quality of the digitizer.

Results

Structure Factor Measurements. The structure factor $S(q)$ for light scattered from the aerosols in the flask as a function of q is shown in Figures 3–5 for three different runs. Zero time corresponds to when the flask was filled from the flame. Due to the rapidity of aerosol coagulation and the manual nature of the OEDC, data close to zero time were difficult to obtain. Figures 3 and 5 were for aerosols in which the flask was well filled. Figure 4 shows an aerosol with roughly $^1/_4$ the concentration, hence $^1/_{16}$ the coagulation rate, as the aerosols in Figures 3 and 5. In all cases the logarithmic $S(q)$ versus q graphs are linear,

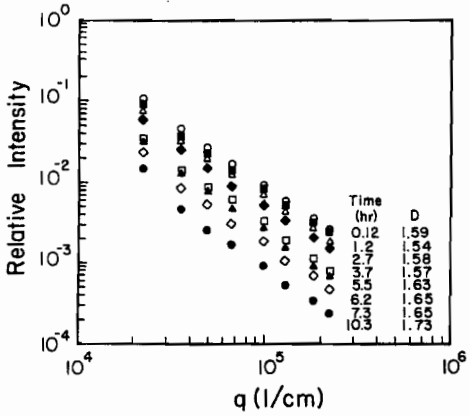

Figure 5. Third aerosol. $D = 1.62 \pm 0.06$; $\lambda = 488$ nm.

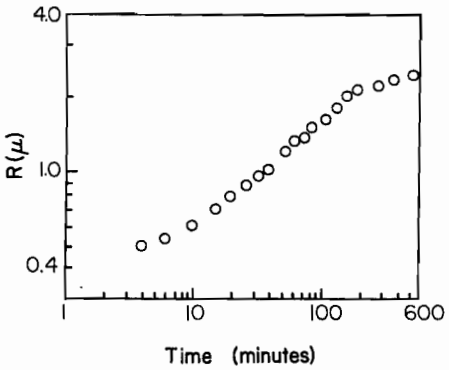

Figure 6. Mean hydrodynamic radius versus time as determined by photon correlation spectroscopy for the aggregating soot aerosol 3.

indicating fractal morphology. Also, while the total intensity decreased slowly with time, probably due to settling or wall losses, the decrease is uniform, so the slope of these curves remains essentially constant. By eq 2 this slope is equal to the negative of the fractal dimension. For the three figures the average fractal dimensions for all times are $D = 1.65 \pm 0.04$, $D \simeq 1.59$, and $D = 1.62 \pm 0.06$ for Figures 3–5, respectively. The overall average of these values is $D = 1.62 \pm 0.06$. Although there is a small systematic trend in D as a function of time in Figure 5, the fact that all the curves have the same shape implies that the fractal morphology once established was maintained during the duration of the agglomeration.

PCS measurements of the intensity-weighted mean hydrodynamic radius for the aerosol in Figure 5 are given in Figure 6. In this aerosol the more powerful argon ion beam was used to make the PCS measurement feasible. The radius R_H increased uniformly from 0.5 to 2.5 μM. Our TEM measurements show the monomer radius to be $a \simeq 10$ nm. Given our q range, 600 nm $> q^{-1} >$ 50 nm, we see the conditions $qR_G > 1$ and $qa < 1$ necessary for eq 2 and the above interpretation to be fulfilled. In a similar manner we point out that our q range is limited to 1 decade. Hence we can only claim the agglomerates are fractal, with dimension D, for 1 decade of size, 600 nm $> q^{-1} >$ 50 nm.

TEM Structure Measurement. Generally speaking, the darkness of a TEM micrograph is not simply proportional to the amount of matter at the point due to the unknown Bragg orientation of the crystallite. However, since there are thousands of monomers in a cluster, it can be reasonably assumed that they are randomly oriented. Thus we may assume the micrograph darkness is proportional to the projected mass thickness of the three-dimensional cluster. Saturation due to extremely large thickness was not a problem.

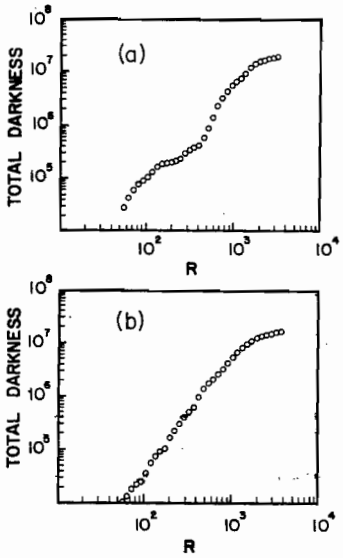

Figure 7. (a) Total integrated darkness within a circle of radius R (arbitrary units) centered on the center of mass of the agglomerate in Figure 2b, point 1. (b) Same as a only the circles are centered as position 2 on Figure 2b, which was chosen to maximize linearity of the graph.

To examine the possible fractal nature of the agglomerate in our micrographs, we used what we shall term the "nested circles" method. This makes use of eq 1 by drawing a series of concentric circles on the digitized two-dimensional projection of the cluster and integrating the image darkness within. This is similar to the original procedure used by Forrest and Witten,[2] who counted the number of monomers within nested squares. The image darkness was assumed to be proportional to the number of monomers or total mass. A log–log graph of this darkness versus the circle radius R will yield a straight line with slope D if the cluster is a fractal.

Tence et al.[14] have recently studied this method of analysis. They have stressed the importance of subtracting the background (noncluster) portion of the micrograph from the cluster darkness before analysis. They have also shown that finite cluster size effects may yield values of D too small by as much as 20%. In our analysis, we have subtracted the background and have examined only large clusters, which were collected near the bottom of the flask after settling.

In our analysis of the micrographs we measured the background darkness with the digitizer at several background points in the picture. An average background darkness was then taken as the average of these randomly selected points multiplied by 1.3 to ensure only the agglomerate was used in the analysis. During the raster scan of the micrograph by the automatic digitizer, digitized points that had a darkness greater than this background were only recorded. In this way the number of recorded points, and hence the amount of computer memory needed, was minimized. Variation of the factor 1.3 from 1.0 to 2.0 did not perceptibility alter the fractal analysis of a given particle.

Another problem which does not seem to have been discussed is a proper method of selecting the center for

(14) Tence, M.; Chevalier, J. P.; Jullien, R. *J. Phys. (Les Ulis, Fr.)* **1986**, *47*, 1989.

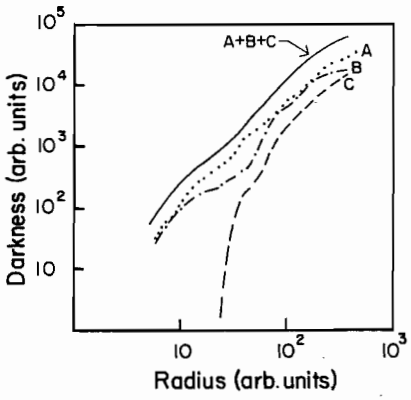

Figure 8. Total integrated darkness for three different clusters, A, B, and C, calculated by using the center of mass for the center of the nested circles. The curve A + B + C is their sum. The slope of this fairly linear sum curve gives $D = 1.72 \pm 0.10$.

the nested circles (or nested squares). A logical and unbiased choice is the cluster center of mass. Figure 7a shows the resultant integrated darkness versus R plot when the center of mass is used as the center of the nested circles for the cluster shown in Figure 2b, point 1. This plot is not very linear, although its rough slope of 1.7 is consistent with our $D = 1.62$ from $S(q)$ measurements. This result is rather typical since the local density near the center of mass may vary widely from cluster to cluster, thus causing a variety of "wiggly" plots such as Figure 7a. In Figure 7b we show results for the same cluster but with a center for the nested circles that has been moved to another point, which optimizes the linearity of the integrated darkness versus R plot. This is point 2 in Figure 2b. Here $D \simeq 1.8$. Such an optimization procedure is similar to that used in earlier work.[2,14]

This analysis and similar analysis of other clusters show us that the fractal analysis and fractal dimension derived therefrom are dependent upon the choice of the center for the nested circles. Our point of view is that no two clusters are identical, and hence each will have a unique integrated darkness versus R plot. The fractal concept is a statistical concept; thus to see the fractal nature, an ensemble average of the particle system must be performed. In fact, this is what occurs in the light-scattering $S(q)$ measurement, since at any given time many aggregates are in the scattering volume.

In Figure 8 we plot the integrated darkness versus R for three different clusters using the nonarbitrary center of mass. Each curve is different than the others and at best only quasilinear. Also shown is the sum of the darkness for all three clusters. This sum represents the ensemble average for this ensemble of three. The average curve is quite linear, indicating fractal morphology, and its slope yields $D = 1.72 \pm 0.1$. This is in fair agreement with the value obtained from the structure factor measurement.

Conclusions

We find that aerosolized carbonaceous soot particles extracted from a flame agglomerate in a room temperature environment to form agglomerates with a fractal morphology. This morphology was seen in both the in situ light-scattering measurements and the TEM analysis. The fractal dimension was found to be $D = 1.62 \pm 0.06$ and 1.72 ± 0.10 for light scattering and TEM, respectively. Thus the agreement between each method is fair. This result suggests there may be small but unidentified systematic errors that are incurred during the sampling and subsequent analysis processes. These experimental values of D are on the low side of the value of $D = 1.7$–1.9 expected for cluster–cluster diffusion-limited aggregation from model simulations.[15-17] A smaller D may be indicative of electrostatic dipolar interactions between particles, as recently proposed for magnetic dipolar particles.[18] We also found that the fractal dimension did not appear to evolve significantly during the coagulation. Finally, we point out that the conditions of our experiment are very similar to those found in practical situations of soot released to a nonturbulent atmosphere; hence our results may apply to these situations of practical importance.

Acknowledgment. We thank K. R. Pohl for assistance in the construction of our optical eight-channel detector. This work was supported by NSF Grants CBT-8603736 and CBT-8709622.

(15) Meakin, P. *Phys. Rev. A* **1984**, *29*, 997.
(16) Jullien, R.; Kolb, M.; Botet, R. *J. Phys. Lett.* **1984**, *45*, L211.
(17) Mountain, R. D.; Mulholland, G. W.; Baum, H. *J. Colloid Interface Sci.* **1986**, *114*, 67.
(18) Mois, P. M.; Botet, R; Jullien, R. *J. Phys. A* **1987**, *20*, L975.